

CHAPTER XIX

BANDWIDTH ENHANCEMENT TECHNIQUES IN PRINTED MONOPOLES FOR ULTRA-WIDEBAND APPLICATIONS IN WIRELESS COMMUNICATION SYSTEMS

TÉCNICAS DE AUMENTO DE ANCHO DE BANDA EN MONOPOLOS IMPRESOS PARA APLICACIONES DE BANDA ULTRAANCHA EN SISTEMAS INALÁMBRICOS DE COMUNICACIÓN

DOI: 10.51859/amplla.sset.2124-19

Helton S. Bernardo ¹

¹ M.Sc. degree student in Electrical Engineering, São Paulo State University (UNESP), School Engineering, São João da Vista, SP, Brazil.

ABSTRACT

With the recent advancements in wireless communication systems, the allocated frequency band spectrum has effectively alleviated congestion for cell phone operators, industrial communication services, and other stakeholders. One potential solution is to explore innovative techniques within mobile devices that facilitate ultra-wideband (UWB) capabilities, enabling a broad spectrum of signal transmission across the communication system. Consequently, simple printed antennas like the $\lambda/4$ -monopole can be utilized to enhance the frequency band width (BW) through appropriate modifications. In this study, we examined three modified antenna models using bulging techniques: conventional, curved-circular, and base-triangular. Comparative analyses were conducted to assess the maximum percentage bands obtained. The results demonstrated a notable increase of 30% to 45% across the models, resulting in a maximum gain of 3.7 dBi. Additionally, it was observed that variations in physical parameters did not significantly impact the bandwidth gain or the radiation pattern.

Keywords: Chamfer and fillet technique. Modified $\lambda/4$ -Monopole. Bandwidth.

RESUMEN

Con la reciente evolución de los sistemas de comunicación inalámbrica, el espectro de banda en frecuencia licenciado ha enfrentado congestiones por parte de operadoras de telefonía celular, servicios de comunicación industrial, entre otros. Una alternativa es la evaluación de técnicas en dispositivos móviles que permitan una banda ultra ancha (UWB) posibilitando una amplia gama de transmisión de señales por el sistema de comunicación. De esta forma, antenas impresas simples como monopolo- $\lambda/4$ pueden actuar para propiciar un alargamiento en la banda en frecuencia (BW) frente a las modificaciones. Este trabajo utilizó tres modelos modificados por técnicas de embaulamiento: convencional, curvo-circular y base-triangular para análisis comparativos entre las máximas bandas porcentuales obtenidas. Los resultados muestran que hay un aumento significativo de 30% a 45% entre modelos, en consecuencia, el máximo ganancia fue de 3.7dBi. Además, los parámetros físicos no afectan la ganancia en banda, ni el patrón de radiación.

Palabras-clave: Técnica de embaulamiento. Monopolo- $\lambda/4$ Modificado. Ancho de Banda.

1 INTRODUÇÃO

The Federal Communication Commission (FCC), a governmental agency in the United States, standardized in 2002 the frequency range of 3.1–10.6 GHz as Ultra-Wideband (UWB) (Saha et al., 2019; Tomar & Kumar, 2015; Ullah et al., 2019). This range is important because it allocates microwave frequencies, most of the bands for wireless communication such as WLANs (2.4—5.6 GHz), mobile phone systems, and satellite communication, among others (Wang et al., 2019). Thus, many planar microstrip antennas can be designed and developed due to their low manufacturing cost, compact size, rapid integration with integrated circuits (IC), and high flexibility.

In Keum and Choi (2018), a set of 16 antenna elements in an array was designed to increase gain for 5G mobile communication systems operating in millimeter waves (30—300 GHz), achieving a frequency band of 4.91 GHz centered at 28 GHz. The well-known technique consisted of inserting U-slots in each patch cell to individually increase the electrical area and achieve a significant gain effect for the radiation pattern. The study demonstrated that the initial antenna element (whose geometry corresponds to the modified monopole) presented a wide frequency band, even at high frequencies, and the addition of other elements in the array caused a considerable increase of approximately 1 GHz in the operating band. In Saha et al. (2019), a modified UWB circular monopole with a pentagonal slot in the center of the antenna was built and designed for high-rate frequency band operation. The printed monopole showed a reflection coefficient $|S_{11}| \leq -10 \text{ dB}$ over a range of 4 – 40 GHz, covering C, X, Ku, K, Ka, and WLAN (Wireless Local Area Network) bands for wireless communications.

In Singh et al. (2016), a Modified Planar Triangular Monopole Antenna (MPTMA) for broadband was studied by modifying a planar-triangular monopole for broadband applications in point-to-point communication systems for medical image processing for heating living tissues. Among the characteristics used in the antenna structure, the Defect Ground Plane (DGP) technique was associated with four antenna models. In these models, the triangular base of the monopole was altered in both the ground plane and the monopole itself. The most promising results demonstrated a frequency band widening (2–8 GHz), increasing 6 GHz of signal transmission for $|S_{11}| \leq -10 \text{ dB}$, with a ratio of 4:1 in terms of bandwidth. The omnidirectional pattern showed a peak gain range of 2 dB to 5 dB at the analyzed frequencies.

In Tomar and Kumar (2015), the design of a modified UWB monopole with a triple band was worked on for applications in WiMAX communication systems (3.3—3.7 GHz), WLAN with IEEE 802.11a standard (5.15—5.85 GHz), and satellite communication in the X band (7.25—8.39 GHz). Among the strategies for the structural arrangement of the monopole, U-slot configurations were used under the microstrip radiator. The bandwidth was drastically increased from 2.8–10.7 GHz.

In Mahmood et al. (2012), a comparative performance analysis of a half-wavelength monopole for WLAN applications (2.4 GHz) with a wideband in UWB was conducted to verify the bandwidth widening behavior along with radiation and efficiency characteristics. In this work, a prototype was built for validation and discussion of simulated and measured results with an omnidirectional radiation pattern.

In Ullah et al. (2019), a high-efficiency UWB monopole antenna operating in microwave frequencies (2.8—22.7 GHz) for image processing communication systems was presented. The technique used, similar to those in other cited works, consisted of the Z-shaped geometric form of the monopole element by impedance matching along the line-resonator junction. The results showed a ratio of 8.33:1 in terms of bandwidth compared to the initial antenna and the proposed one. The radiation efficiency values increased from 70% to 93%, considering the evaluated models. Finally, the radiation pattern was analyzed at various frequencies of the achieved bandwidth, with a realized gain between 1.6—6.4 dBi.

In Wang et al. (2019), U-slot and EBG (Electromagnetic-Bandgap) structural elements were inserted into a typical conventional circular UWB monopole to widen the frequency band for the allocation of frequencies from 2.6 to 12.9 GHz, encompassing WLAN bands (4.8—5.9 GHz) and the X band allocated for satellite downlink communication. It was found that these U-slots, after insertion, create operating signal transmission bands in the frequency response and allow filtering of other bands generated by the EBG elements added in the ground plane. It was also found that the position and physical size of the EBG, as well as the lengths of the slots, determined the location of these bands in the response (by frequency shift).

According to Balanis (2016, p. 218), a monopole (linear wire segment) with a length of $\lambda/4$ exhibits an electromagnetic behavior described by the field equations, in particular, the electric field component given by the amplitude in eq. (1):

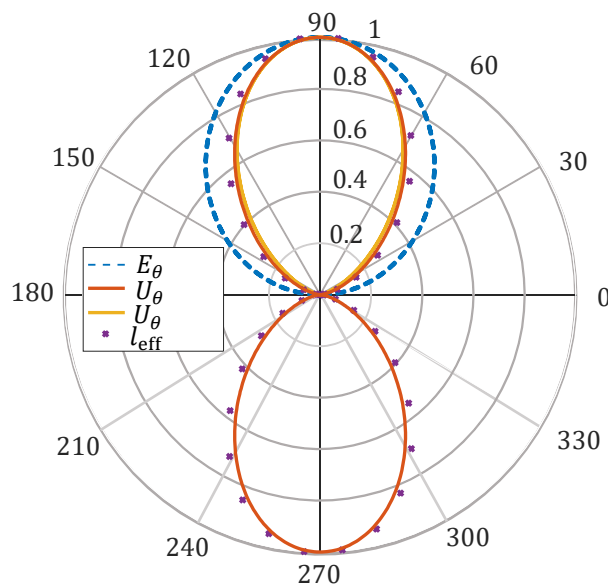
$$E_{\theta} = \frac{E_0 \cos\left(\frac{\pi}{2} \cos \theta\right)}{\sin \theta}, H_{\phi} \approx \frac{E_{\theta}}{\eta}. \quad (1)$$

Where E_{θ} is the amplitude of the normalized electric field in the θ -direction in spherical coordinates (blue curve in Fig. 1); E_0 is the amplitude of the normalized electric field in [V/m] in the International System (SI); H_{ϕ} is the approximation of the amplitude of the magnetic field in the ϕ -direction valid in the far field, when the electromagnetic waves present plane wave fronts, and η is the intrinsic impedance of the medium. In the far field, $k_0 l \gg 1$ (k_0 is the propagation constant and l is the length of the monopole wire), the radiation intensity, U_0 , can be calculated by (2):

$$U_0 = E_{\theta}^2 \sim B_0 \sin^3 \theta. \quad (2)$$

Where B_0 is an amplitude given in W/sr (unit of power per unit solid angle), and the approximation corresponds to the square of the electric field component by expression (1). The graphical behavior can be seen in Fig. 1, according to the orange and yellow curves for normalized and approximated U_{θ} .

Figure 1 – Theoretical radiation pattern for a typical monopole ($l = \lambda/4$).



Source: The author.

The effective length, l_{eff} , of the $\lambda/4$ monopole in the θ -direction computed by (3):

$$l_{\text{eff}} = -a_{\theta} \left(\frac{\lambda}{\pi}\right) \cos\left(\frac{\pi}{2} \cos \theta\right). \quad (3)$$

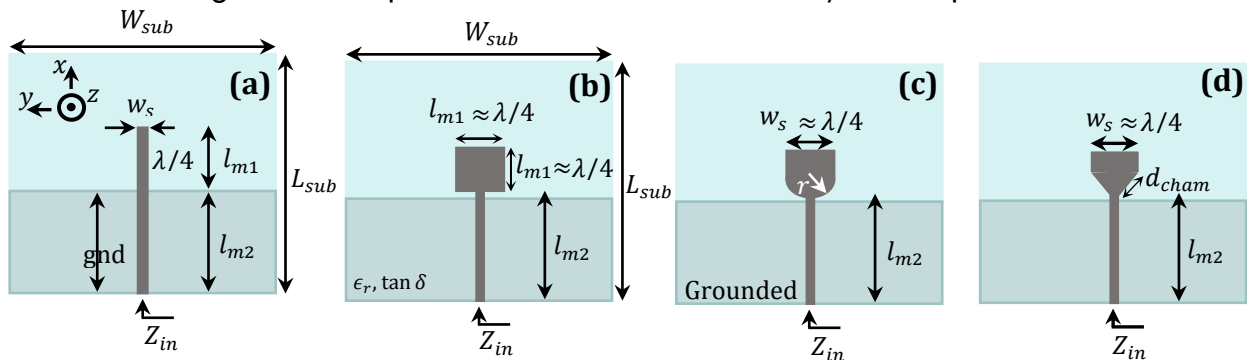
The maximum [meter] amplitude of the effective length is given by the ratio λ/π and decreases with the increase of the elevation angular position θ . In Fig. 1, it is

possible to verify the dashed purple curve demonstrating the theoretical behavior. Finally, it is worth noting that Fig. 1 presents a strictly omnidirectional radiation pattern (in two directions, one of them is broadside, that is the signal propagation, $\theta = 90^\circ$).

2 PLANAR STRUCTURES PROPOSED FOR MONOPOLES

Figure 2(a) depicts a $\lambda/4$ -monopole antenna with dimensions based on (Falcão, Felício, & Peixeiro, 2023), whose dielectric used was the substrate for FR-4, $\epsilon_r = 4.4$, $\tan \delta \approx 0.09$. In Figure 2(a), the $\lambda/4$ -monopole with $l_{m1} = \lambda/4$ is inserted into the substrate with a height $h = 1.6$ mm, initial width $w_s = 3$ mm, and $gnd = 80$ mm (coinciding with the value l_{m2}). In Figure 2(b), a small rectangular base with a square shape of length $\lambda/4 \times \lambda/4$ is inserted, increasing the electrical area of the monopole (modified model 1). In Figure 2(c), there is a modification to the rectangular-square base with a curved shape with a certain radius $r = 1$ mm (initial), from then on, the bulging technique is applied (modified model 2). Finally, in Figure 2(d), the same modification is introduced with a triangular base with a distance $d_{cham} = 8$ mm (initial) between the monopole feed line and the modified square base (modified model 3). The input impedance used for the insertion of the monopoles was initially calculated at theoretical values for $Z_{in} \approx 50 \Omega$. All values are depicted in Table 1.

Figure 2 – Proposed structures for modified $\lambda/4$ -monopole antennas.



Source: The author.

Table 1 – Parameters used (physical and dielectric).

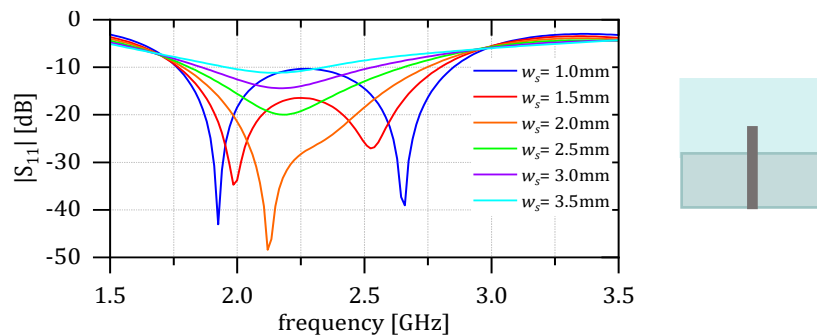
W_{sub}	L_{sub}	w_s	l_{m2}	l_{m1}	gnd	h	d_{cham}	r
$1,1\lambda$ (150mm)	$1,1\lambda$ (150mm)	Varies (1— 3.5mm)	$0,52\lambda$ (75mm)	Varies (20— 28mm)	$0,56\lambda$ (80mm)	0,011 λ (1.6mm)	Varies (8— 12mm)	Varies (1— 15mm)

Source: The author.

3 CONVENTIONAL MICROSTRIP LINE PRINTED MONOPOLE

For the conventional model presented in Figure 2(a), the reflection coefficient and input impedance were simulated against a parameterization of the linear monopole width. A preliminary study was conducted for the ground plane length and fixed at $gnd = 0.56\lambda$ through parameterization. The reflection coefficient is shown in Figure 3:

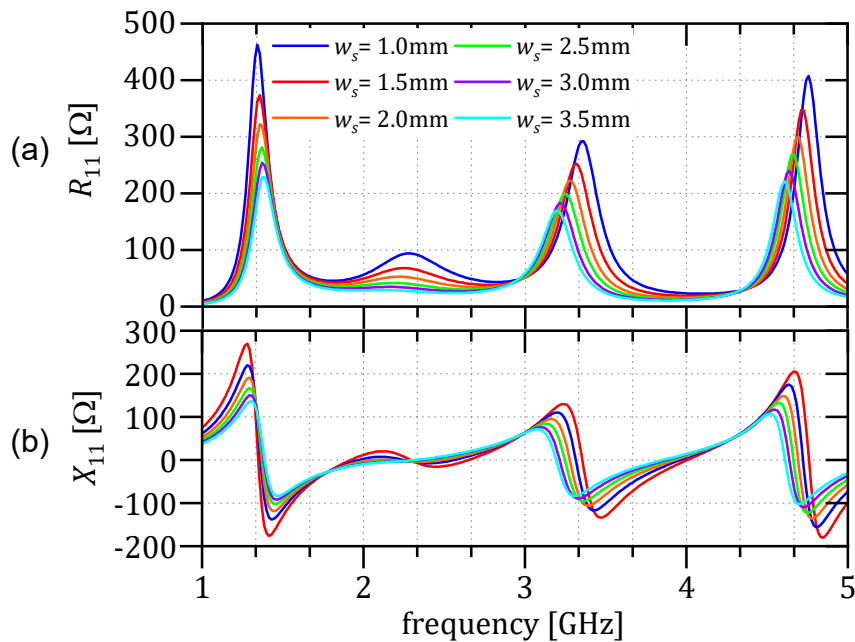
Figure 3 – Reflection coefficient altering the width of the conventional monopole.



Source: The author.

One notices a relation of bandwidth increase in $|S_{11}| \leq -10$ dB for smaller width values. In $w_s = 1$ mm, it is possible to verify two well-separated operating modes (in frequency), thus being a dual-band region for resonance frequencies of 1.93 GHz and 2.6 GHz. However, as the interest is in a full bandwidth across a wider spectral region, the bandwidth $w_s = \{1.5; 2.0\}$ mm is interesting because it allows for a closer approximation of the resonant modes, enabling signal transmission stability for the resonance frequencies of 1.99 GHz and 2.53 GHz ($BW \sim 1.04$ GHz). It is observed that the set of bandwidth values $w_s = \{2.5; 3.0; 3.5\}$ mm already reduces the bandwidth and consequently inhibits one of the resonant operating modes, causing the reflection coefficient to become unsatisfactory $|S_{11}| \geq -10$ dB ($BW \sim 0.405$ GHz for $w_s = 3.5$ mm), impairing impedance matching. In Figure 4, the reflection impedance at frequency $Z_{11}(f)$ of the conventional monopole associated with the input resistance R_{11} and input reactance X_{11} is presented, as highlighted in Figures 4 (a) and 4 (b), this parameter can provide information about antenna matching. It is noted that for a frequency window of 1–5 GHz, there are four resonances $f_r \sim \{1.4; 2.3; 3.3; 4.7\}$ GHz approximately. In these resonances, it can be seen that the peaks of resistances R_{11} show maxima at values of smaller width of the printed monopole in the resonant behavior of the expected reactance $X_{11} \approx 0\Omega$, which means that the antenna matching is adequate, albeit with a high impedance value associated.

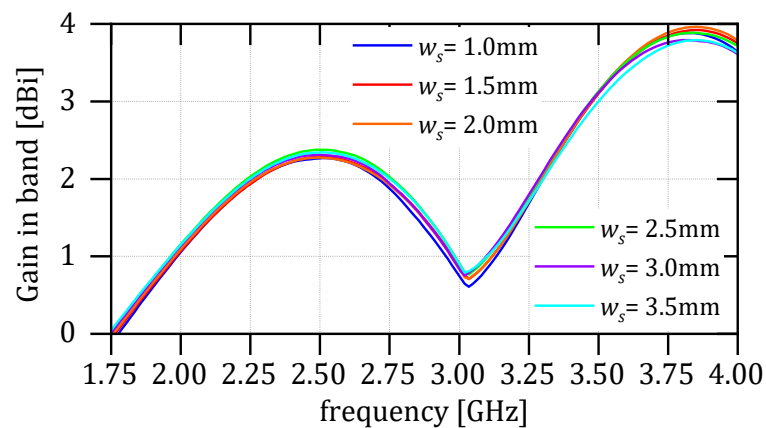
Figure 4 – Complex impedance $Z_{11}(f)$ versus changes in w_s of the conventional monopole.



Source: The author.

Through parameterization simulation, it was possible to verify the bandwidth gain characteristics as shown in Figure 5. The theoretical conventional gain is approximately 5 dBi for monopole antennas, as depicted in the illustration of Figure 5; this increase occurs at higher frequencies. From the graphical analysis, the maximum obtained at 2.5 dBi was at 2.5 GHz for a 500 MHz bandwidth (2.55–2.75 GHz). Another relevant point extracted from this analysis is that the physical width w_s does not influence the radiation pattern, especially the gain, as illustrated in Figure 7. The minimums and maximums of the electric field amplitude are analyzed in Figure 6, as indicated by the blue color for absence of field and the red color for electric field amplitude for maximum magnitudes at the resonance frequency of 2.1 GHz. The field configuration $|\mathbf{E}|$ allows for the propagation of two wavefronts radiating part of the electrical energy (open circuit) associated with the surface current distribution \mathbf{J}_s .

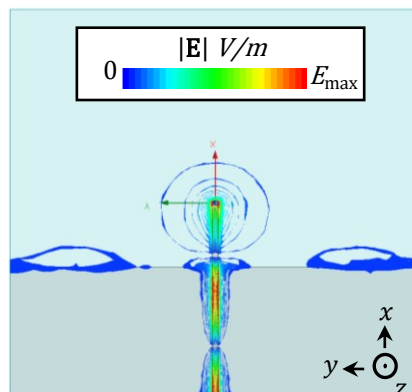
Figure 5 – Gain in bandwidth of the conventional monopole.



Source: The author.

In Figure 6, for visualization of the field distribution, the physical width w_s was set to 3mm.

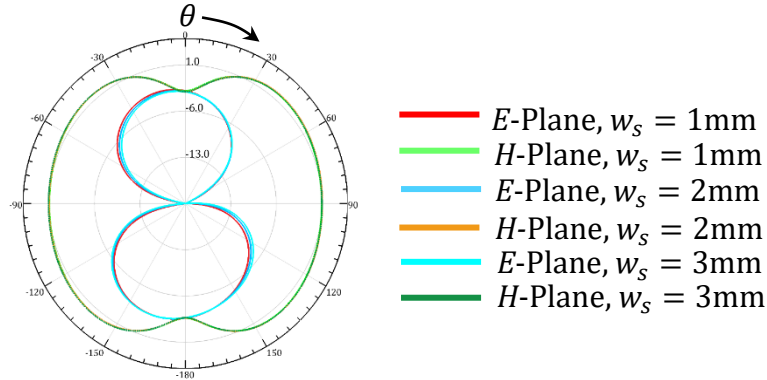
Figure 6 – Magnitude distribution of electric field $|\mathbf{E}|$ of the conventional monopole.



Source: The author.

Finally, observations about the effects of physical width on radiation pattern for gain are possible. As depicted in Figure 7, the E -planes (formed by the director vector of the electric field component and maximum broadside propagation direction) and H -planes (formed by the director vector of the magnetic field component and maximum broadside propagation direction) are explored for selected widths in $w_s = \{1, 2, \text{ and } 3\}$ mm. It is evident that w_s does not have a direct influence on radiation in the plane of spherical positions $(\theta, \phi = 90^\circ)$. The radiation pattern exhibited bidirectionality in the E -plane and omnidirectionality in the H -plane.

Figure 7 – Radiation pattern for gain changing w_s of the conventional monopole.

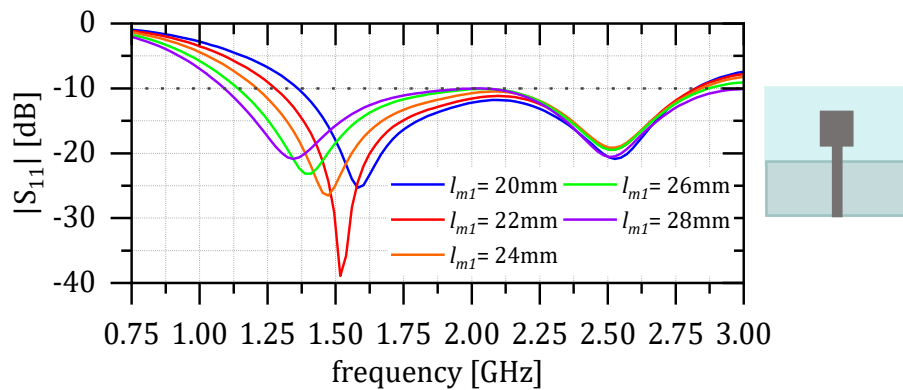


Source: The author.

4 MODIFIED MONOPOLE WITH SQUARED FORMAT

The first modification associated with the conventional model given in Figure 2(b) is the insertion of a square base element. The variations (increase) in the length of the side l_{m1} cause an increase in the frequency bandwidth BW , as observed in Figure 8 associated with the reflection coefficient.

Figure 8 – Reflection coefficient with respect to the alteration of l_{m1} of modified monopole 1.

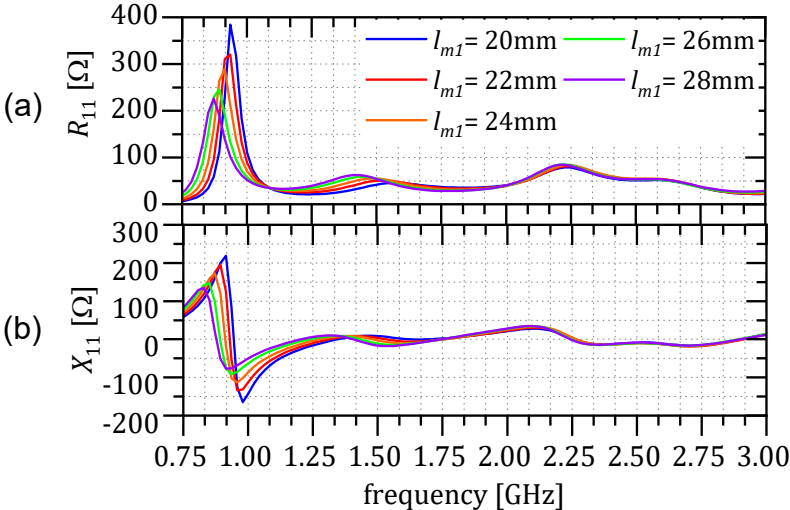


Source: The author.

The increase in the lateral length l_{m1} (20—28mm) provided an increment of 300MHz in the bandwidth (blue curve to violet curve). The smallest estimated percentage bandwidth was 70% (blue curve), while the maximum simulated percentage bandwidth was 91% (violet curve), taking the resonance frequency $f_r \sim 2.1$ GHz. The problem with increasing l_{m1} is related to the introduction of separation between modes, causing the wide frequency band with $l_{m1} = 20$ mm to be split into two independent bands at $l_{m1} = 28$ mm, as indicated by the trend in the curves in Figure 8. In Figure 9(a), it is observed that the operating modes that predominated in Figures

4(a—b) are drastically reduced in magnitude (remaining below 100 Ω) when viewed from 1.25GHz. In Figure 9(b), the same process occurs as described previously. The predominance of the modes is given by the resonance $f_r \sim 0.9\text{GHz}$.

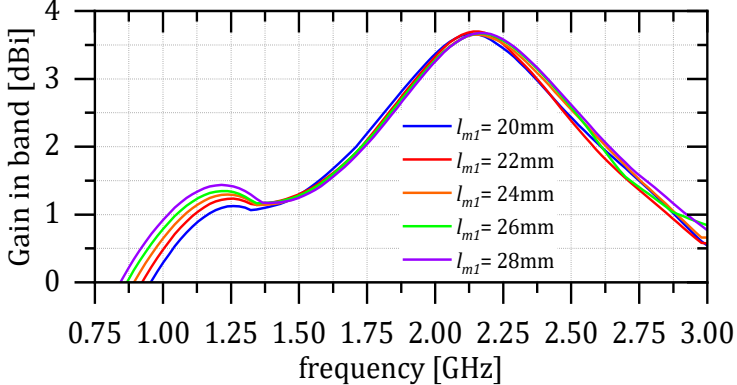
Figure 9 - Complex impedance $Z_{11}(f)$ with respect to the alteration of l_{m1} of the modified model 1.



Source: The author.

It is observed that a peak gain in the band at 2.16GHz was maintained, presenting a maximum value of 3.7dBi. For gain values greater than 3dB, the percentage bandwidth in terms of gain is 23.8% (with $BW \sim 0.5\text{GHz}$).

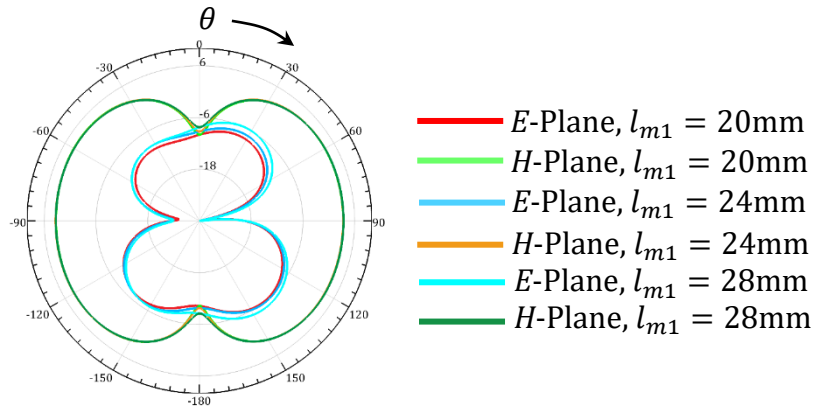
Figure 10 – Band gain with respect to the alteration of l_{m1} of the modified monopole 1.



Source: The author.

The radiation pattern remains unchanged with the variations in l_{m1} . The addition of the base does not significantly alter the spectral distribution of radiated power (still exhibiting bidirectionality in the E -plane and omnidirectionality in the H -plane) as highlighted in Fig. 11.

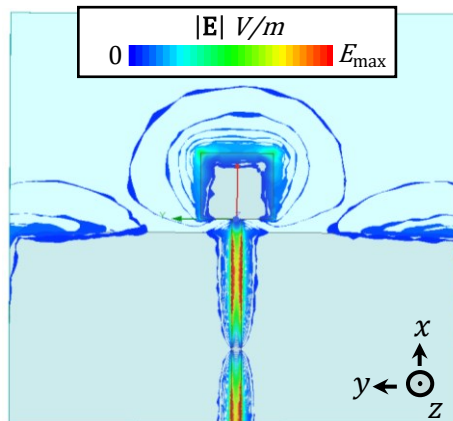
Figure 11 - Radiation pattern with respect to the alteration of l_{m1} of the modified monopole 1.



Source: The author.

Fig. 12 presents a more uniform distribution at the ends of the monopole, with the maxima of the electric field shown on the surface of the monopole (in red). With the increase in the effective area, two regions (in green) of maxima of $|E|$ appear on the square base, associated with the electrical path of the surface current J_s .

Figure 12 – Electric field magnitude distribution $|E|$ of the modified monopole 1.

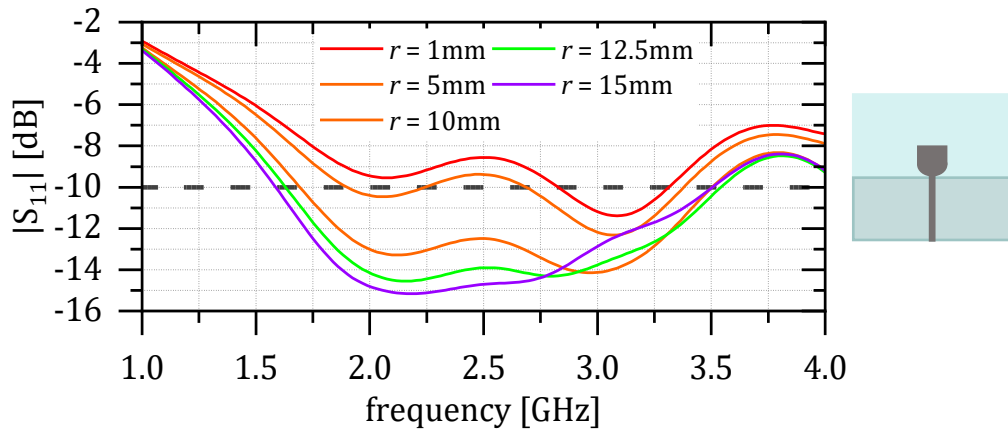


Source: The author.

5 MODIFIED MONOPOLE BY CURVED-CIRCULAR BULGING

The modification of the square base element of the monopole (model 1) by curved-circular bulging causes an increase in the frequency band in a range of 1.5–3.5GHz, allowing an increase of approximately 2GHz for the reflection coefficient $|S_{11}| \leq -10dB$, as highlighted in Fig. 13:

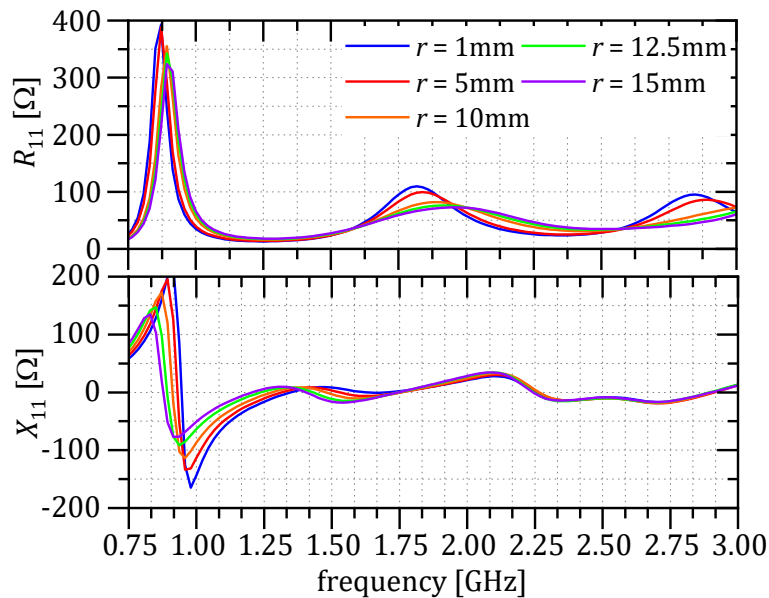
Figure 13 – Reflection coefficient with respect to the alteration of the radius r of modified monopole 2.



Source: The author.

It was found that the radial increase r from 1 to 15mm causes a broadening (as observed in the trend from the red curve to the purple curve). The widest operating bandwidth analyzed (corresponding to the purple curve) was 1.58–3.51GHz, for 15mm from larger values for r , no such increase was observed. In Fig. 14(a-b), the reflection impedance Z_{11} is shown as a function of the radial change in curved-circular curvature.

Figure 14 - Complex impedance $Z_{11}(f)$ versus variation in r of modified monopole 2.

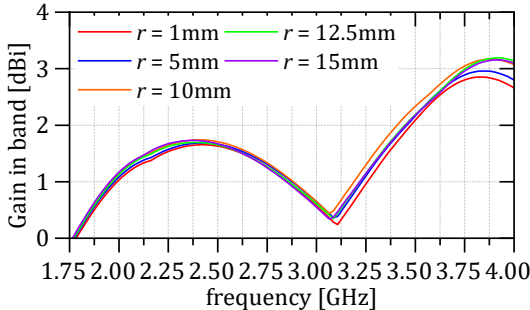


Source: The author.

From Figure 14(a), it is noted a predominant mode with a peak of high resistance and a characteristic resonant effect in Figure 14(b) in the analysis of reflection

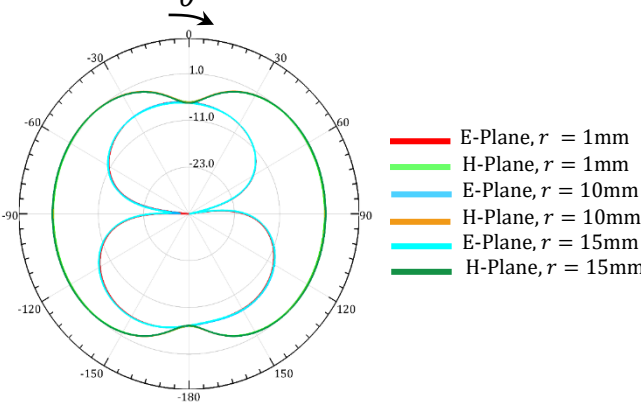
reactance at the frequency of 0.915 GHz, indicating resonant points away from the design frequency. Additionally, slight entries of the next operating modes at 1.5, 2.1, and 2.75 GHz are highlighted. At these resonances, the system's energy may be distributed and among the operating modes. It was found that the circular curvature radius decreases the peaks of input resistance R_{11} , smoothing them, similarly to the characteristic curve of reflection reactance X_{11} . Figures 15 and 16 present the radiated characteristics of the antenna (modified model 2) for bandwidth gain and spatial gain in elevation θ , respectively.

Figure 15 – Bandwidth gain versus radius r alteration of the modified monopole 2.



Source: The author.

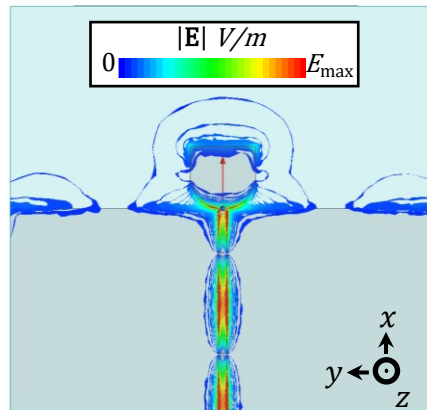
Figure 16 – Radiation pattern for gain versus radius r alteration of the modified monopole 2.



Source: The author.

Figure 15 is very similar to the behavior of Figure 5, with a slight global drop of 0.5dB in the observation window of Figure 15. The parametric effect of the curvature radius r does not influence the gain pattern in the band and, as seen in Figure 16, also does not impact the radiation pattern, maintaining the same bidirectional (E -plane) and omnidirectional (H -plane) format when three curves $r = \{1, 5, \text{ and } 15\}$ mm are selected. Figure 17 shows the electric field distribution $|E|$ in amplitude for the frequency of 2.1GHz and $r = 15$ mm. In blue colors, the electric field amplitude is zero, in contrast to the orange-red colors, where the electric field amplitude is maximum E_{max} , as illustrated in Figure 17:

Figure 17 – Distribution in magnitude of the electric field $|\mathbf{E}|$ of the modified monopole 2.



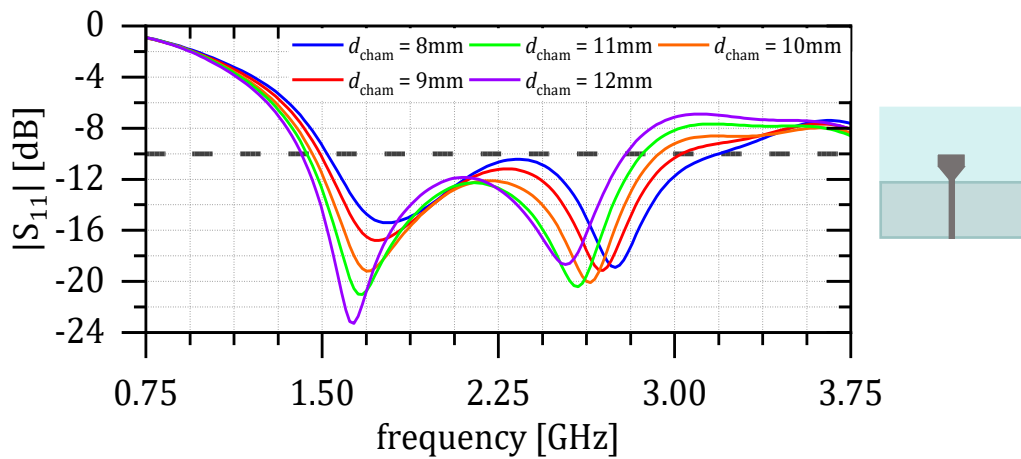
Source: The author.

The distribution demonstrates uniformity along the feed line of the monopole. Two clear field nulls are noted, reaching the resonant element, and a distributed concentration of the electric field in the circular curvature is confirmed. This can be explained, in fact, by the volumetric density of electromagnetic energy associated with the electric field u_E , which is proportional to the square of the electric field $|\mathbf{E}|$, that is, $u_E \sim \varepsilon_{\text{eff}}|\mathbf{E}|^2/2$ (Balanis, 2016).

6 MODIFIED MONOPOLE WITH RECTILINEAR CURVE

Finally, the behavior of the modified monopole (model 3) was analyzed using the chamfering technique with a straight curve (triangular base) as described in Fig. 2(d). This analysis was conducted by varying the physical chamfering distance of the inserted element in Fig. 2(b), denoted as d_{cham} . The relationship between bandwidth and chamfer distance is evaluated in Fig. 18, showing an increase in bandwidth with a decrease in d_{cham} . It is possible to see two modes in operation very close together, leading to a broadening of the bandwidth as typically seen in Fig. 3 for the blue curve, anticipating the mutual excitation of these two modes.

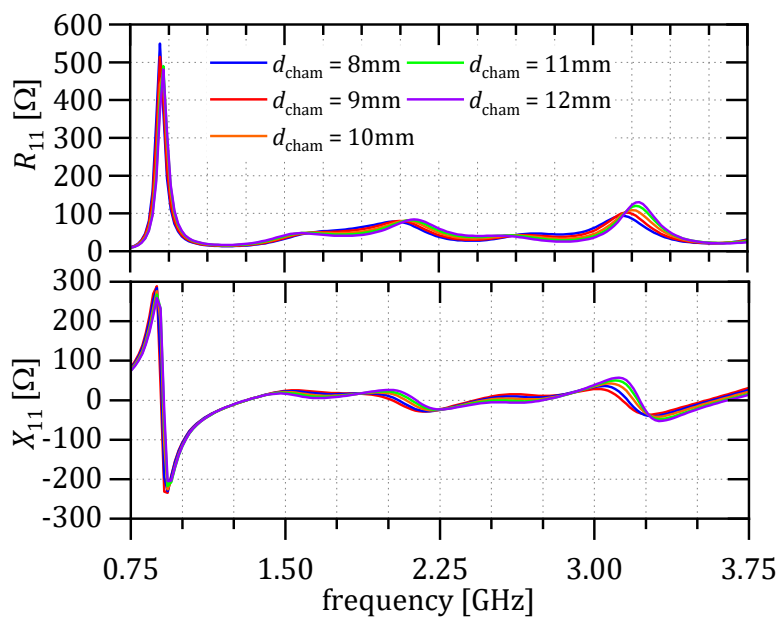
Figure 18 – Reflection coefficient versus the variation of d_{cham} of the modified monopole 3.



Source: The author.

Numerically, the bandwidth approached that of the monopole with curved chamfering. The largest bandwidth observed was ($BW \sim 1.5\text{--}3.2\text{GHz}$), 300MHz lower compared to the bandwidth of the circularly chamfered monopole. Subsequently, the effect of matching is described by the reflection impedance Z_{11} as d_{cham} varies, as shown in Fig. 19 (a—b).

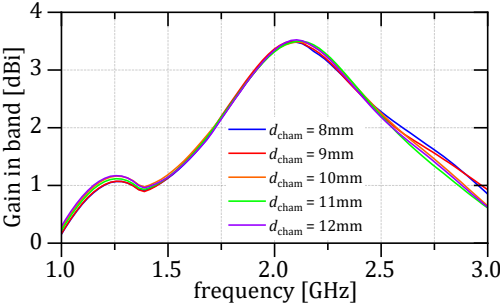
Figure 19 – Complex impedance $Z_{11}(f)$ versus the variation of d_{cham} of the modified monopole 3.



Source: The author.

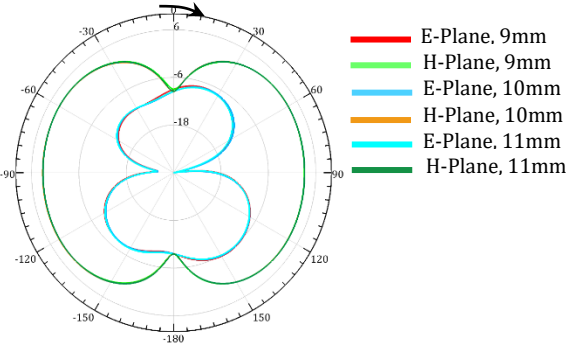
In practical terms, there is still a predominant resonance at 0.915GHz in the frequency response for both resistance (Fig. 19 (a)) and reactance (Fig. 19 (b)) of reflection. At 2.1GHz, a slight entry of the operating mode is observed in both graphs with maximum resistance peaks of approximately $R_{11} = 100 \Omega$ and a slight shift of the resonance at the center of the reactance curve $X_{11} \approx 0 \Omega$. Regarding the antenna gain for the modified model 3, it was analyzed through Figs. 20 and 21 that the physical parameter d_{cham} does not significantly interfere, as depicted in Figs. 20-21. The gain in band (frequency response) is maximized at 2.1GHz to 3.5dBi, varying considerably from the gain compared to the curved-circular chamfer (Fig. 15), which shows two frequency moments of maximization.

Figure 20 – Bandwidth gain versus d_{cham} alteration of the modified monopole 3.



Source: The author.

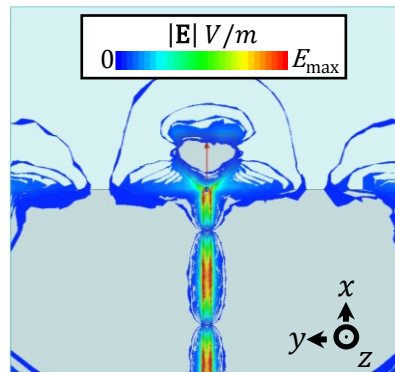
Figure 21 – Radiation pattern for gain versus d_{cham} alteration of the modified monopole 3.



Source: The author.

Figure 21 shows an unchanged radiation pattern (gain) in response to the variation of the chamfer distance, with three selected values $d_{cham} = \{9, 10, \text{ and } 11\}$ mm. The *E*-plane and *H*-plane had a bidirectionality and omnidirectionality associated with spatial gain (for angular elevation θ), respectively, without significant changes. Figure 22 demonstrates the same procedure for the uniform distribution of the electromagnetic signal reaching the monopole, indicated by the two nulls in the color transition from blue to red.

Figure 22 – Magnitude distribution of the electric field $|E|$ of the modified monopole 3.



Source: The author.

As explained earlier, part of the electromagnetic energy resides in the curvature of the bulge (with lower intensity indicated by the green shading), resembling the behavior of the curved-circular bulge described in the previous section. As emphasized, this electric field (in amplitude) promotes resonance at the operating frequency of 2.1 GHz.

7 CONCLUSION

In summary, it can be stated that the implementation of the bulging technique promoted a significant increase of 30% in the bandwidth in the conventional model (Conv.) of the quarter-wavelength monopole to modification 1 (Mod. 1), as established in Table 2. The maximum bandwidth is observed in modification 2 (Mod. 2) at 84.4%, with a lower gain of 1.8 dBi at the resonance frequency $f_r = 2.1$ GHz, being the model with the most suitable matching $R_{11} = 1.192Z_0$ (59.6Ω). It is possible to establish relationships between BW and the studied physical parameters as described in Table 2.

Table 2 – Comparison between all models ($*Z_0 = 50 \Omega$).

Models	BW [%]	Gain [dBi]	Rel. BW and physical params.	$R_{11} [Z_0]^*$ (em f_r)
Conv.	46,0	2,5	$\uparrow BW \downarrow w_s$	$1,870Z_0$
Mod. 1	76,8	3,7	$\uparrow BW \uparrow l_{m1}$	$1,684Z_0$
Mod. 2	84,4	1,8	$\uparrow BW \uparrow r$	$1,192Z_0$
Mod. 3	73,1	3,5	$\uparrow BW \downarrow d_{cham}$	$1,682Z_0$

Source: The author.

ACKNOWLEDGMENTS

This work was carried out with the support of the Coordenação de Aperfeiçoamento de Pessoal de Nível Superior - Brazil (CAPES) – Financing Code 001.

REFERENCES

- Falcão, P., Felício, J. M., & Peixeiro, C. (2023). Wideband, wearable, printed monopole antenna system for integration into an electromagnetic radiation evaluation device. *Sensors*, 23(7), 3667. <https://doi.org/10.3390/s23073667>.
- Keum, K., & Choi, J. (2018). A 28 GHz 4 × 4 U-slot patch array antenna for mm-wave communication. In: 2018 International Symposium on Antennas and Propagation (ISAP 2018), 1–2. Busan, Korea.
- Mahmood, F., Ali, S. M. U., Alam, M., & Willander, M. (2012). Design of WLAN patch and UWB monopole antenna. In B. S. Chowdhry, F. K. Shaikh, D. M. A. Hussain, & M. A. Uqaili (Eds.), *Emerging Trends and Applications in Information Communication Technologies. Communications in Computer and Information Science* (Vol. 281, pp. 295–304). Springer Berlin Heidelberg. http://link.springer.com/10.1007/978-3-642-28962-0_29.
- Saha, T. K., Goodbody, C., Karacolak, T., & Sekhar, P. K. (2019). A compact monopole antenna for ultra-wideband applications. *Microwave and Optical Technology Letters*, 61(1), 182–186. <https://doi.org/10.1002/mop.31519>.
- Singh, S. K., Sharma, M. P., & Kashyap, N. K. (2016). A modified planar triangular monopole antenna for wide band applications. In: 2016 11th International Conference on Industrial and Information Systems (ICIIS), 598–602. Roorkee, India: IEEE. <http://ieeexplore.ieee.org/document/8263009/>.
- Tomar, S., & Kumar, A. (2015). Design of a triple band-notched UWB planar monopole antenna. *Journal of Microwaves, Optoelectronics and Electromagnetic Applications*, 14(2), 184–196. <https://doi.org/10.1590/2179-10742015v14i2514>.
- Ullah, S., Ruan, C., Sadiq, M. S., Haq, T. U., & He, W. (2019). High-efficient and ultra-wide band monopole antenna for microwave imaging and communication applications. *Sensors*, 20(1), 115. <https://doi.org/10.3390/s20010115>.
- Wang, Y., Huang, T., Ma, D., Shen, P., Hu, J., & Wu, W. (2019). Ultra-wideband (UWB) monopole antenna with dual notched bands by combining electromagnetic-bandgap (EBG) and slot structures. In: 2019 IEEE MTT-S International Microwave Biomedical Conference (IMBioC), 1–3. Nanjing, China: IEEE. <https://ieeexplore.ieee.org/document/8777856/>.